Peer-reviewed version available at *Materials* **2019**, *13*, 111; doi:10.3390/ma13010111

Article

Perfect Combination of LBL with Sol-Gel Film to Enhance the Anticorrosion Performance on Al Alloy under Simulated and Accelerated Corrosive Environment

Xia Zhao [1,2,3,4*], Zuquan Jin [2*], Shuai Yuan [1,2], Binbin Zhang[1,3], Nazhen Liu[1,2,3], Shibo Chen[5], Shuan Liu[1,3], Xiaolin Sun[2] and Jizhou Duan [1]

[1] Key Laboratory of Marine Environmental Corrosion and Bio-fouling, Institute of Oceanology, Chinese Academy of Sciences, Qingdao 266071, China
[2] Cooperative Innovation Center of Engineering Construction and Safety in Shandong Blue Economic Zone, Qingdao University of Technology, Qingdao 266032, China
[3] Open Studio for Marine Corrosion and Protection, Pilot National Laboratory for Marine Science and Technology, Qingdao 266235, China
[4] Center for Ocean Mega-Science, Chinese Academy of Sciences, Qingdao 266071, China
[5] School of Chemistry and Chemical Engineering, Guangxi University, Nanning 530004, China
* Correspondence: zx@qdio.ac.cn (X.Z.); zuquanjin@126.com (Z.J.)

Abstract: Given of the outstanding versatile properties, the multilayered anti-corrosion coatings have drawn great interests in academic and engineering fields. However, the application of multilayered coatings is restricted by some limitations such as low interlayer compatibilities, harsh preparation process, etc. This work introduced a composite film fabricated on 2A12 aluminum alloy surface, including an anodic oxide film, a sol-gel film as well as a layer-by-layer (LBL) self-assembling film from bottom to top. The microstructure and elemental characterization indicated that the finish of the coating with the LBL film resulted in a closely connected multilayered coating with a smoother surface. The anticorrosion performance was systematically evaluated in the simulated corrosive medium and neutral salt-spray environment. The intergrated coating with the LBL film presented an excellent anticorrosion ability with the system impedance over 10^8 Ω•cm^2 and the self-corrosion current density two orders of magnitude lower than that of the other coatings. After the acceleration test in salt-spray environment, the multilayered coatings could still show a good protective performance with almost no cracks and no penetration of chloride ions. It is believed that the as-constructed multilayered coating with high corrosive properties and fine surface state will have promising applications in the field of anticorrosion engineering.

Keywords: multilayer; corrosion; impedance; layer-by-layer

1. Introduction

Aluminum and its alloys are widely used in the fields of shipbuilding, oceanography engineering, aerospace and machine manufacturing because of its low density, low thermal expansion coefficient, high strength and strain performance [1-2], which have drawn much attention of both researchers and engineers as promising materials for electrical appliances and machinery industry [3-8]. Under certain circumstances, Al alloys possess some anticorrosion resistance because of the naturally formed oxidized thinner film [9-10]. However, the oxide film is thin and inhomogeneous, once encountered high moisture, high salt and other impurities factors, it would

Peer-reviewed version available at Materials 2019, 13, 111; doi:10.3390/ma13010111

corrode first from the weak spots, such as voids or cracks. So the natural oxide film could not offer sufficient protection to the underlying metal under long-term exposure in harsh environments. Localized corrosion might take place in the environment containing chloride ions, resulting in enormous financial cost or even catastrophic safety accident [11-12].

In order to improve the corrosion resistance and stability of the Al alloys, more protective technologies need to be explored to extend its service life in the marine environment [13-14]. There are two typical approaches to improve the corrosion resistance of Al alloy, one is to ameliorate the element proportion of Al alloys, and the other is to cover a protective film on the surface of Al alloys. At present, artificial fabricated films upon Al alloy substrates are commonly used to improve the protective ability, including anodic oxidation [15-16], laser cladding [17], sol-gel method [18], self-assembly technology [19] and anticorrosion coatings [20] etc.

Sol-gel method is regarded as an effective and environmentally friendly coating sealing technology. This method has the advantages of low costs, simple operation, and low reaction temperature. Dense and porous film can be obtained from this technology, which can prolong the service life and enlarge the application of Al alloys in the marine environment [21-25]. However, due to improper reaction conditions in the heat treatment process, film could crack and initiate the consequent degradation of the protective film [26]. Therefore, it is extremely urgent to enhance the anti-cracking performance of the sol-gel film, so as to improve its anticorrosive ability.

Recently, a layer-by-layer (LBL) self-assembly method has been developed as a promising technique for synthesis of composite functional film with evident advantages, such as simplicity, versatility and controllability etc., attracting great interest of researchers as a strategy for creating anticorrosion films [27]. The functional film is composed of polyelectrolyte multilayers, which are formed by constructing the polyelectrolyte with positive and negative charges through electrostatic adsorption layer by layer onto the metal surface [28-30]. LBL self-assembly technique is based on the consecutive adsorption of polyanions and polycations via electrostatic interactions [23, 31, 32]. By applying LBL self-assembly technique, polyelectrolyte molecules could adsorb to the sol-gel film, repairing the surface defects such as cracks and holes by electrostatic adsorption, thereby obviously improving the protective performance of the film. Therefore, the combination of these two methods was investigated to improve the anti-corrosion properties of Al alloy. In present, limited research about the combined technologies can be found, compared to the single protective film with some micro cracks, which increases the potential risk of corrosion in the future service.

In this paper, anticorrosive coatings were fabricated on Al alloy substrate, combining and utilizing the advantages of LBL and sol-gel method. A porous oxide film, a pore-sealing sol-gel film, and an LBL self-assembly film were successively prepared. Surface morphologies, composition as well as surface roughness of the films were comprehensively characterized, and the protective mechanism of the films was speculated. Equivalent circuits were established to simulate the anticorrosion performance of different films in NaCl solutions and the electrochemical parameters were obtained. The morphologies and composition was compared after the salt-spray test of the protective films to evaluate the long-term performance.

2. Experimental and characterization

2.1. Materials and reagents

The major elemental composition of Al alloys 2A12 are (wt. %): Si 0.5, Cu 3.8-4.9, Mg 1.2-1.8, Zn 0.3, Mn 0.3-0.9, Ti 0.15, Al balance. The material has a thickness of 3–4 mm and was purchased from Beijing Goodwill Metal Technology Co., Ltd. Acetone, ethanol were obtained from Sinopharm Chemical Reagent Co., Ltd. Poly (ethyleneimine) (PEI) with a MW of 70 kDa, and GO of 1 wt. % were purchased from Shanghai Aladdin Bio-Chem Technology Co, Ltd. Poly (acrylic acid) (PAA) with a MW of 450 kDa was purchased from Sigma-Aldrich. All the reagents were of analytical grade and used without further purification. Deionized water with a resistivity of 18.0 uS/cm was used in all the experiments.

Peer-reviewed version available at Materials 2019, 13, 111; doi:10.3390/ma13010111

2.2. Pretreatment and preparation of anodic oxide film

The Al alloy samples were hand-cut and punched. They were polished by grinding wheel and premilling machine. A natural oxide film was formed by alkali washing in the air. Then the samples were ultrasonic cleaned with absolute ethyl alcohol and washed with distilled water. Finally, they were polished with diamond polishing agent and dried with an air blower.

In the anodization experiment, the Al alloy sample was connected to the positive pole and the platinum electrode was connected to the negative pole of a power source. The electrolyte for the anodization experiment contains 40 g/L oxalic acid, the anodizing voltage was 55 V, the oxidation current density was less than 2 A/dm^2, and the anodization time was 60 min. Ice water bath was used to guarantee the constant temperature of the electrolyte. After washed with deionized water and dried with cold air, the anodized film on Al alloy was obtained. The samples were placed in a desiccator for storage.

2.3. Preparation of the sol-gel film

Alumina sol was firstly prepared as follows: 2 g of aluminum isopropoxide was added to 50 mL n-propanol under continuously stirring until the aluminum isopropoxide was completely dissolved. Then, 2 ml of acetylacetone and distilled water were synchronously added under stirring. Finally 3-5 drops of nitric acid as stabilizer were added to the above solution, and then stirred for 2 h on a magnetic stirrer and aged for 24 h to obtain a clear and transparent alumina sol.

The sol-gel film was further prepared on the surface of the Al alloy with anodic oxide film. The anodized Al alloy sample was suspended perpendicularly to the surface of the alumina sol and immersed in the sol at a uniform rate. And the sample was allowed to stay for 1 min in the sol to ensure that the prepared sol-gel film was uniform. The sample was then pulled out from the alumina sol at a rate of about 20 mm/min, and a layer of sol-gel film was successfully covered on the Al alloy surface. The sol was quickly converted into a wet gel in the atmosphere. The sample was heated under 120 ℃ for 30 min and then cooled at the room temperature. This operation was repeated for six times to improve the corrosion resistance of the sample.

2.4. Preparation of the LBL self-assembled protective film

The Al alloy sample sealed with sol-gel film was immersed in a beaker containing 4 mg / L polyethylenimine (PEI) for 5 min, and dipped in distilled water for 2 min. The sample was subsequently placed into a beaker containing 4 mg / L polyacrylic acid (PAA) for 5 min and also dipped in distilled water for 2 min. This procedure was called one cycle, which was repeated for 10 times in total. And the polyethyleneimine and polyacrylic acid LBL self-assembled protective film, marked $(PEI/PAA)_{10}$, was obtained. And the whole procedure of film preparation was illustrated in Fig.1.

2.3. Methods

2.3.1. Characterization

Scanning electron microscopy (SEM) (Hitachi S-3400N, Japan) and atomic force microscope (AFM) (Multimode 8, Bruker) were employed to observe surface morphology of the samples. The samples for SEM determination were sputtered with gold. The elemental analysis was characterized by energy dispersive X-ray spectrum (EDS). Atomic force microscopy (AFM) measurements were performed at room temperature in the air and operated in tapping mode. The scanning area of AFM measurement was 10 μm×10 μm and 1 μm×1 μm. The chemical compositions were measured by XPS (ESCALAB250Xi, Thermo Scientific, Waltham, USA). The spectra were recorded with monochromatized Al kα radiation (1486.6 eV) as the excitation source with a base pressure of 1.3×10^{-9} mbar, at a constant power of 150 W (15 kV,10 mA). The pass energy was 20 eV for the high-

Peer-reviewed version available at Materials 2019, 13, 111; doi:10.3390/ma13010111

resolution spectra. The binding energy of adventitious carbon (C1s: 284.8 eV) was used as a basic reference.

2.3.2. Electrochemical measurements

EIS measurements were performed using a P 4000+ electrochemical workstation. A classical three-electrode cell system was employed, in which a saturated calomel electrode (SCE) was used as the reference electrode, a platinum plate was used as the counter electrode and the Al alloy samples were used as the working electrode, respectively. EIS measurements were performed over the frequency range from 100 kHz to 10 mHz. The EIS data was analyzed and fitted by electrical equivalent circuit models using the ZSimpWin software.

2.3.3. Salt-spray Test

The neutral salt spray test was conducted to evaluate the corrosion resistance of different samples covered with anodic oxide film, sol-gel film and LBL self-assembling film according to GB/T 10125 standard in a salt spray chamber (SUGA CYP-90, Japan). 5 wt. % NaCl solution with pH 6.5 ~7.2 was used as media, and the test temperature was (35±2)℃. The spray pressure was between 0.1 and 0.15 MPa, and the inlet pressure was between 0.2 and 0.4 MPa. The panels with the size of 20×20×3 mm^3 were placed in the chamber at an angle of 45°. Three duplicate specimens were tested for different film samples. The interval between each specimen was above 5 mm to avoid interaction. The morphology of the panels was recorded by a digital camera every 24 hours, and the total experiment period was 168 hours.

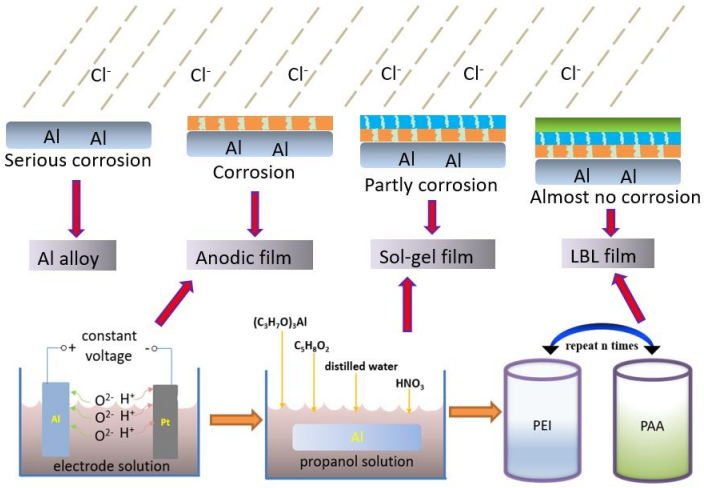

Figure 1. Schematic of the construction for protection film on Al alloy.

3. Results and discussion

3.1. Surface morphologies and composition of the films

Fig.2 showed the typical SEM images of a blank Al alloy and the different resultant films. On the surface of the untreated Al alloy(Fig.2a), numerous scratches and irregular porous structures were observed. The heterogeneous structure with special dislocations stress can induce higher increment of pitting corrosion [33], so, further treatment was needed.

The uneven surface of the Al alloy substrate was improved after the anodization process (Fig.2b). The enlargement image showed that the surface was covered with a porous film, accompanied by some waves, which could be due to the simultaneous growth and dissolution during the anodization process. Although the anodic oxide film could produce certain protection on the substrate, the corrosive ions would stay in the microporous structure and cause local corrosion being exposed to the corrosive medium. Thus, some sealing methods were needed for improving the anticorrosive

Peer-reviewed version available at Materials 2019, 13, 111; doi:10.3390/ma13010111

performance of the film. Fig.2(c) showed the surface morphology of a sol-gel film, which was prepared on the surface of the anodic oxide film. Except for some non-uniform bulk materials, a homogeneous surface with less micropores was observed on the sol-gel film. The better surface state indicated that the setting temperature of drying heat treatment was appropriate during the preparation process of sol-gel film. The aluminum sol could penetrate into the micro-pores and cracks of the anodic oxide film by physical adsorption, and then filled and sealed the defects. The sealing effect was obvious and the anticorrosive ability of Al alloy was expected to be improved. However, it can be seen that the sol-gel film was not ideal. Some slight cracks still existed on the surface, which could be due to the volatilization of organic molecules dissolved in the sol-gel solution in the process of drying and heat treatment and film shrinkage.

Fig. 2(d) showed the surface morphology of the LBL self-assembly film, it was covered with a relatively uniform and dense material, some waved structure and defects, such as cracks and pores, was not observed. The surface of film was smoother and more uniform than the other films. The polyanion-electrolyte ions was successfully absorbed and covered on the surface of the sol-gel film by self-assembly technology. The compactness of the film was improved, which could protect Al alloy from the corrosive medium directly, and then, enhance its anticorrosion performance. According to the EDS results, the content of C element in LBL film was increased by 4 times comparing with that of sol-gel film. The N element, which was not included in other films, appeared in the LBL film with the content of 9.08 %, indicating the existence of PEI. For the content of Al, it decreased from 25.85 % in sol-gel film to 0.31 % in LBL film, which suggested that the LBL film was almost completely covered on the sol-gel film and the Al alloy was isolated from the outside environment. It was concluded that polyelectrolyte solutions including a certain concentration of PEI and PAA can be used to prepare polyelectrolyte multi-layer composite films by chemical absorption, and it was expected to be an effective method for Al alloy protection.

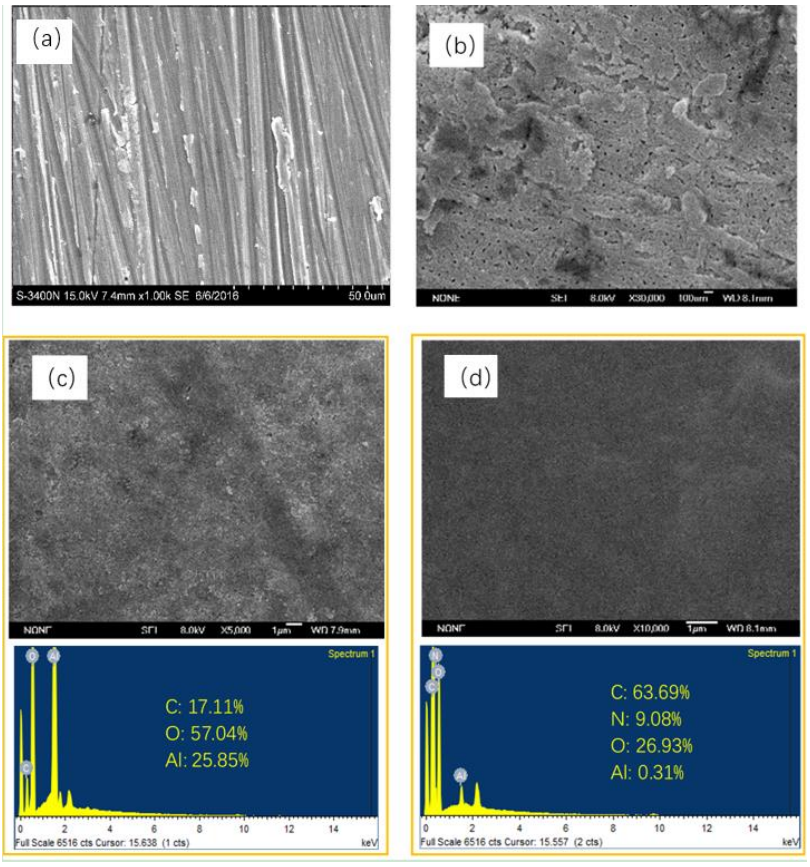

Figure 2. SEM images and EDS results of (a) bare Al alloy, (b) anodic oxide film,(c) sol-gel film and (d) LBL film.

Peer-reviewed version available at Materials 2019, 13, 111; doi:10.3390/ma13010111

3.2. Chemical composition of different films

XPS technology was utilized to analyze the chemical composition of different films on Al alloy substrate. Figs.3 a-c revealed the XPS survey spectra, as well as fitted curves for Al2p, O1s, C1s or N1s for the anodic oxide film, sol-gel film and LBL assembled film, respectively.

The XPS survey spectrum of the anodic oxide film sample (Fig.3a) mainly proved the presence of Al and O on the surface of film with the atomic fractions 21.19 % and 44.81 %, respectively. The characteristic peak of O1s was strong, which indicated the composition of aluminum oxide. The peak binding energy of O1s was 530.70 eV, corresponding to the combination of oxygen in Al_2O_3 with the form of O^{2-} ions. The Al2p peak binding energy was corresponding to the combination of Al^{3+} ions in Al_2O_3 with a binding energy of 73.76 eV.

The XPS survey spectrum of the sol-gel film sample mainly illustrated the presence of C, Al and O on the surface of sol-gel film, as depicted in Fig. 3b. The main elements on the surface of protective film were observed as O, Al and C, and the atomic fraction was 51.64 %, 24.12 %, and 24.07 %, respectively. There were a few changes in binding energy of O1s peak and Al2p peak of the sol-gel film, comparing with that of the anodic oxide film. The C1s peak binding energies were 284.60 eV, 283.40 eV, and 286.00 eV, corresponding to the C-O, Al-O-C, and C-H bonds. The content of Al and O had less increment than that of the anodic oxide film. In addition to the element C, the amounts of the other impurity elements were relatively decreased, which illustrated the sol-gel film was well combined with the anodic oxide film and played a certain role of filling and sealing.

The XPS survey spectrum of the LBL assembled film sample showed the presence of C1s, N1s and O1s, with almost no Al element was detected. The characteristic peaks of C1s, N1s, and O1s were rarely strong, and the atomic fractions were 65.90 %, 13.28 %, and 18.72 %. The electron binding energy of oxygen was 531.00 eV, corresponding to the C-O bond. The electron binding energy of N element was 397.90 eV and 399.50 eV, corresponding to the C-N and NH_2-R bonds. The binding energy of C element was 283.50 eV，283.90 eV and 284.80 eV, corresponding to the C-H, CH_2 and C-O bonds, which came from PEI and PAA, respectively. It was demonstrated that the LBL self-assembled film was successfully covered on the sol-gel film. No aluminum element was detected, indicating that the self-assembled film was entirely deposited onto the sol-gel film, and played a good sealing effect for the base material, which could prevent penetration of the corrosive ions and provide ideal protection for Al alloy.

Peer-reviewed version available at Materials 2019, 13, 111; doi:10.3390/ma13010111

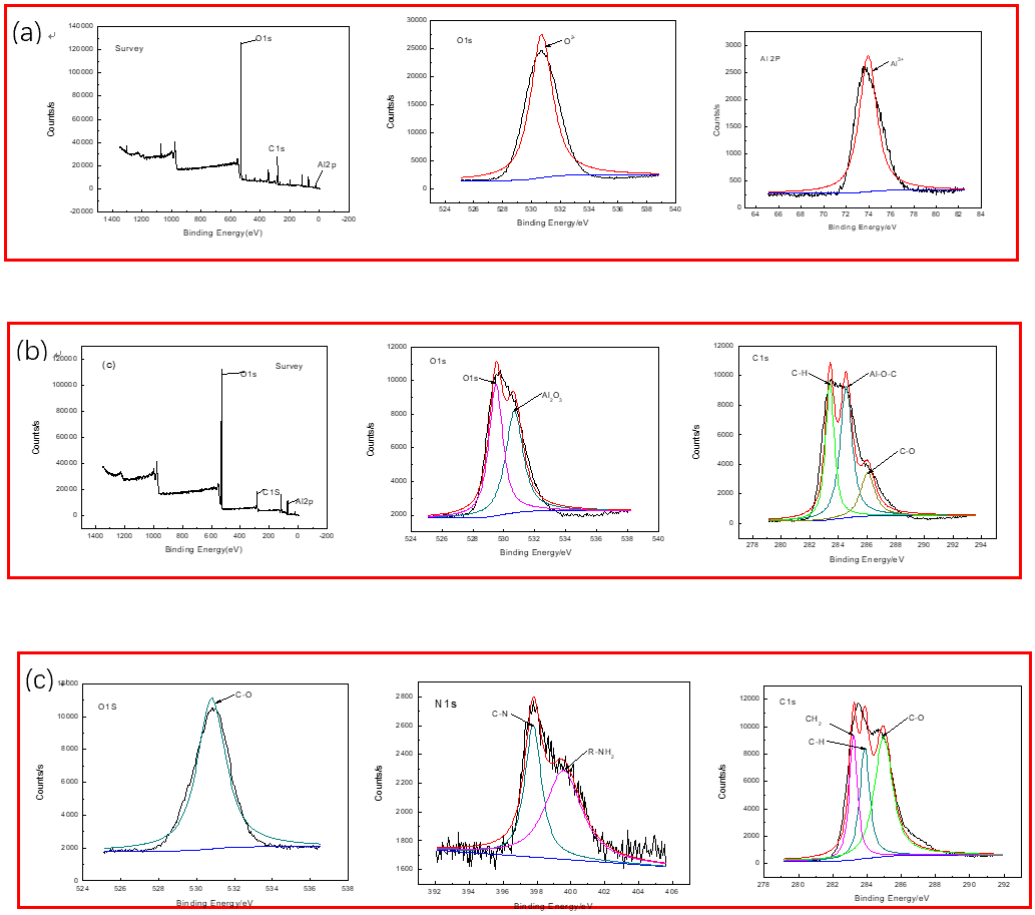

Figure 3. XPS spectrum of different films: (a) anodic oxide film, (b) sol-gel film and (c) LBL film.

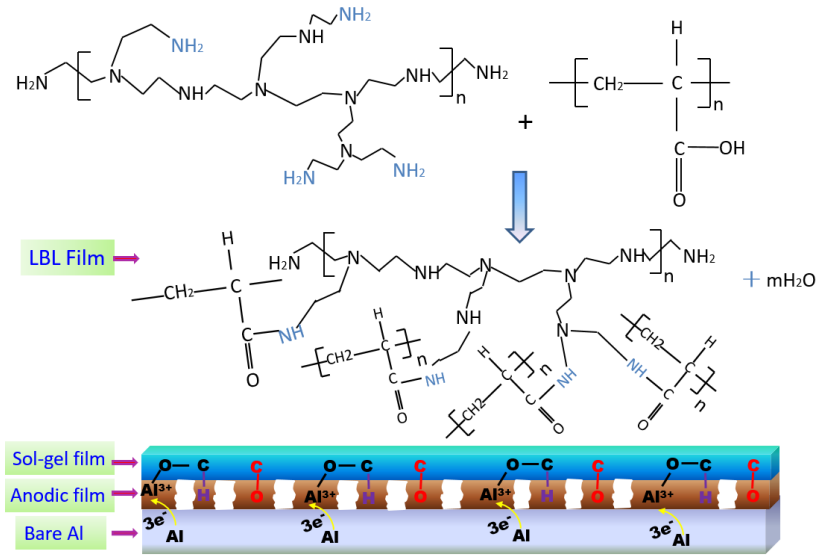

Figure 4. Schematic diagram of protection mechanism.

From the XPS results it could be speculated that Al atom could release three electrons and transformed into Al^{3+}, participating to the formation of O-Al-C bond, and then improved the adhesion ability of the anodic oxide film. As several functional groups were existed in PAA, such as hydroxyl, carboxyl and carbonyl, the chemical bonds in LBL sample were different from those of sol-gel film under the influence of the electron cloud density in functional groups. A large number of carboxyl groups in polyacrylic acid could react with the amino group to form O=C—NH—C group, which

Peer-reviewed version available at Materials 2019, 13, 111; doi:10.3390/ma13010111

endow LBL film with more stability than sol-gel film. The reaction diagram of the protective mechanism for different films was illustrated in Fig. 4.

3.3. surface roughness

The AFM scan in Fig. 5 showed the topography of different films. Fig. 5 (a) was the AFM morphology of bare Al alloy surface, which included the surface height of the sample [33]. The higher of the surface, the lighter of the color on the graph. It could be observed that the surface of Al alloy substrate was uneven and covered with some scratches. The difference between the highest and lowest location was 948.00 nm, indicating that the naturally formed anodic oxide film was irregular and disordered.

Fig. 5 (b) was AFM of Al alloy immersed in the oxalic acid system for some time. The morphology revealed that the film surface was also uneven but the polishing marks disappeared, indicating that a layer was grown on the Al surface accompanying with some lamellar and step-like structures. The peak-valley difference was 363.90 nm, which was smaller than that of the Al alloy matrix. Therefore, the as-prepared anodic oxide film was successfully covered on the surface of Al alloy substrate, and it would endow Al alloy with certain protective ability for preventing the corrosion medium.

Fig. 5(c) showed the AFM morphology of the sol-gel film. The peak-valley difference was about 245.10 nm, which was smaller than that of the Al alloy substrate and the anodic oxide film. Scratches, cracks as well as other visible defects were significantly reduced. The sol-gel film had changed the surface state of the anodic oxide film with a lot of small yurts replacing the lamellar and stepped structures. It maybe because that some small molecules in the sol-gel materials could penetrate into the based film and fill the porous and micro-cracks, and then, the surface roughness would be reduced and the corrosion resistance of the substrate was improved.

Fig. 5(d) showed the AFM map of LBL film. From the morphology it could be seen that the peak-valley difference was about 152.00 nm, and the film was more smooth and flat than that of the other films. Almost no pore structures could be observed by naked eyes. As the water-soluble polyelectrolyte was deposited alternatively from the anions to cations, positive and negative charges were adsorbed on the surface of the film by electrostatic binding force. The formed self-assembled film was dense, uniform and smooth. The surface roughness was the smallest, which could play an ideal protection for Al alloy matrix.

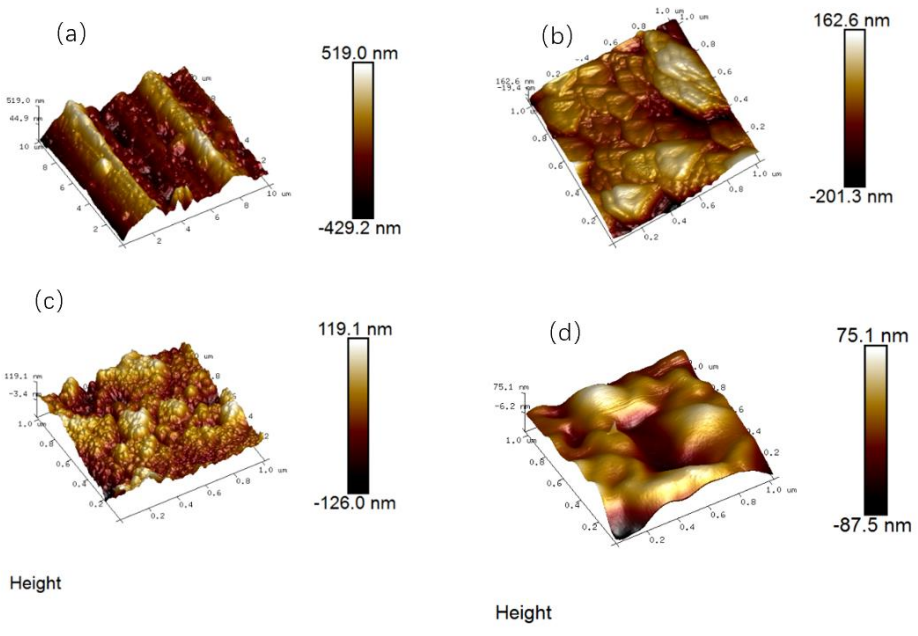

Figure 5. AFM tapping mode 3D images of (a) Al alloy, (b) anodic oxide film, (c) sol-gel film and (d) LBL film.

Peer-reviewed version available at Materials 2019, 13, 111; doi:10.3390/ma13010111

3.4. Anticorrosion properties

The anticorrosion performance is a key factor in evaluating the possibilities of the protective film in fundamental research and practical applications [27]. The electrochemical behaviors of four different samples, such as, the blank Al alloy, Al alloy with anodic oxide film, sol-gel film and LBL film were determined in 3.5 wt. % NaCl solution, individually, and the results were illustrated in Fig.6.

In Fig.6, it can be seen that the radii of the capacitive arc for four types of samples were different, indicating various protective abilities of the protective films. For blank Al alloy sample, it was the smallest, followed by anodic oxide film, sol-gel film and LBL samples. Meanwhile, in Fig.6b, the total system impedance followed the law of blank sample, anodic oxide film, sol-gel film and LBL film. Especially for LBL film, the system impedance was higher than $10^8\Omega\bullet cm^2$, indicating an excellent protective performance than the other films. For phase angle in Fig.6c, except blank Al alloy sample, all the other samples presented multi time-constants features. Fig.7 showed the diagram of equivalent circuit models used for fitting the measured EIS data, and the fitted results were illustrated in Table 1. For blank Al alloy, the Nyquist spectrum presented only one capacitive semicircle. The surface of blank Al alloy was abraded by the SiC sand paper, and no film was formed on the metal surface, therefore, the characterization of the determined curve was the charge-transfer process at the solution/alloy interface. Thus, the corrosion parameters should be fitted by model 1, and the code could be described as $R_s(Q_{dl}R_{ct})$. R_s denoted the solution resistance, Q_{dl} and R_{ct} represented the double-layer capacitance, and the charge-transfer resistance of the interfacial double electric layer, respectively. Specially, in this work, the entire constant phase elements Q were used to model the capacitance because of the heterogeneity of the electrode surface. The impedance of Q is expressed as

$$Z_Q = \frac{1}{Y_0(j\omega)^n} \quad (1)$$

Herein, Y_0 and n are the coefficient and the exponent, respectively, ω is the angular frequency in rad s^{-1} ($\omega = 2\pi f$), and j is the imaginary unit with j^2=-1 [35-36]. For Anodic oxide film, the curve in Fig.6(a1) showed a depressed capacitive semicircle. Essentially, the semicircle was formed by two overlapping semicircles, located at high frequency and low frequency, respectively, which were related to two electrochemical processes. The high-frequency semicircle was associated with the anodic oxide film, whereas the low-frequency semi-circle was corresponded to the charge-transfer process. Because there were numerous defects in the anodic oxide film as shown in Fig.2b, the corrosive medium could penetrate the anodic oxide film directly through these cracks into the film/metal interface, and then, result in various series connections of these two electrochemical processes, as displayed by model 2 in Fig.7. In addition, the total model code could be expressed as the series circuit $R_s(Q_cR_c)(Q_{dl}R_{ct})$, of which, Q_c and R_c were the capacitance and resistance of the protective film, respectively.

For sol-gel film, although the system impedance was higher than that of the anodic oxide film, the layer could not play a good protection role because of the small amount of micropores. Thus, Model 2 was also employed to imitate sol-gel film with two electrode processes.

For LBL film, the system impedance reached $1.32\times10^8\ \Omega\bullet cm^2$, which were significantly higher than that of the other films, suggesting that the corrosive ions could be effectively inhibited from participating in the electrochemical reaction[37], that is, the LBL film could provide great protective effect for base metals. And from Fig.6(c), it can be seen three time constants presenting in Bode plots for LBL film. So, the protective LBL layer should be regarded as a capacitor in the analyzing process of EIS plots and the model code could be denoted as the parallel circuit $R_s(Q_{LBL}(R_{LBL}(Q_cR_c)(Q_{dl}R_{ct})))$.

In summary, the total impedance of the three models could be calculated by the following equations:

$$\text{Model 1:}\quad Z_1 = R_s + \frac{1}{\frac{1}{R_{ct}} + Y_{0dl}(j\omega)^{n_1}} \quad (2)$$

Peer-reviewed version available at Materials 2019, 13, 111; doi:10.3390/ma13010111

$$\text{Model 2: } Z_2 = R_s + \frac{1}{\frac{1}{R_c}+Y_{0c}(j\omega)^{n^2}} + \frac{1}{\frac{1}{R_{ct}}+Y_{0dl}(j\omega)^{n1}} \quad (3)$$

$$\text{Model 3: } Z_3 = R_s + \frac{1}{Y_{0LBL}(j\omega)^{n_3}+\frac{1}{R_{LBL}+\frac{1}{\frac{1}{R_c}+Y_{0c}(j\omega)^{n^2}}+\frac{1}{\frac{1}{R_{ct}}+Y_{0dl}(j\omega)^{n1}}}} \quad (4)$$

The fitted results were illustrated in Table 1. Once the surface of Al alloy was covered with different films, the electrochemical parameters changed accordingly. Obviously, the changing law of R_c value followed the order of LBL > sol-gel > oxide film > blank Al alloy. The lowest R_c value of blank Al alloy indicated that the erosion process occurred more easily comparing to the other samples, indicating that corrosion was prone to be induced in this material. R_c value increased as LBL films were deposited on sol-gel film, confirming the fact that the polyelectrolytes could remedy the defect of sol-gel film and enhance its protection ability. Corrosive medium could be separated effectively by LBL self-assembling film, and cannot penetrate into the Al alloy through LBL film to cause corrosion. Generally, the inhibition efficiency (η) can be obtained from R_{ct} by the following formula[38]:

$$\eta = \left(1 - \frac{R_{ct}^0}{R_{ct}}\right) \times 100\% \quad (5)$$

where R^0_{ct} signifies the charge transfer resistance of pure Al alloy, and R_{ct} represents the charge transfer resistance of Al alloy with different protection film.

According to the results of η illustrated in Table 1, the united coating containing sol-gel layer and LBL film owned the highest inhibition efficiency, which was 98.1%, indicating a remarkable corrosion resistance performance. These results further proved that LBL film could combine perfectly with sol-gel film and then obtained a protective film with excellent resistance to external erosion.

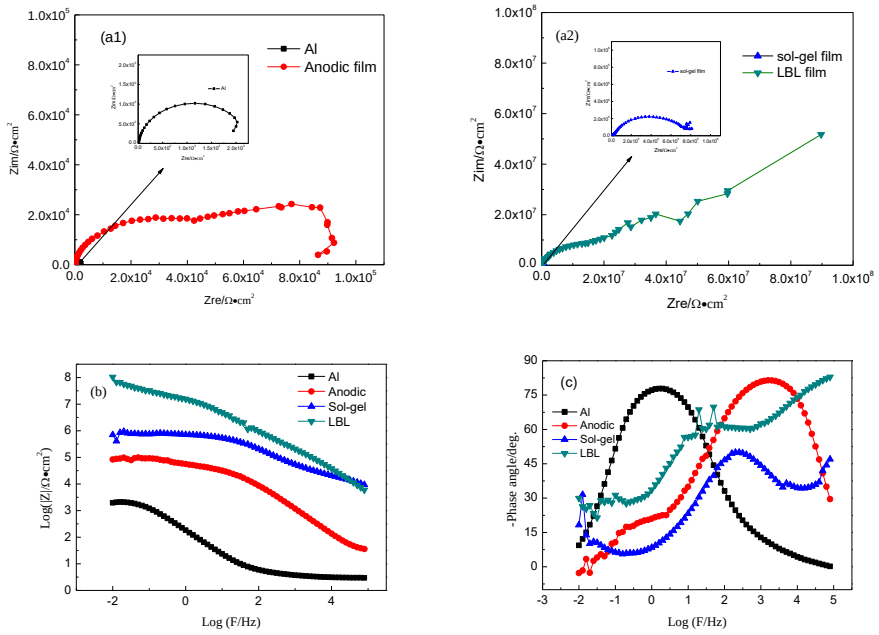

Figure 6. EIS plots and the fitting curves of Al alloy samples with different film. (a1) and (a2) Nyquist plots; (b) and (c) Bode plots.

Peer-reviewed version available at Materials 2019, 13, 111; doi:10.3390/ma13010111

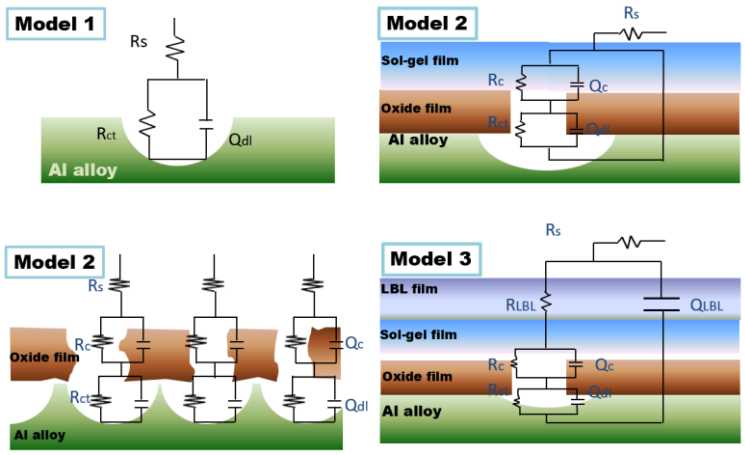

Figure 7. Equivalent models of EIS plots for Al alloy samples with different films.

Table 1. Fitting results of EIS for Al alloy with different films.

Sample	Q_{dl}		R_{ct}	Q_c		R_c	Q_{LBL}		R_{LBL}	η
	Y_{0dl} $\Omega^{-1}cm^{-2}s^n$	n	Ω cm^2	Y_{0dl} $\Omega^{-1}cm^{-2}s^n$	n	Ω cm^2	Y_{0LBL} $\Omega^{-1}cm^{-2}s^n$	n	Ω cm^2	%
Al alloy	0.00106	0.88	2446	\	\	\	\	\	\	
Oxide film	2.95×10^{-7}	0.93	3.25×10^{4}	5.94×10^{-6}	0.83	6.29×10^{4}	\	\	\	92.5
Sol-gel film	4.42×10^{-9}	0.75	3.58×10^{4}	4.74×10^{-8}	0.69	7.54×10^{5}	\	\	\	93.2
LBL film	0.76×10^{-11}	0.93	1.30×10^{5}	0.79×10^{-10}	0.87	9.03×10^{6}	0.45×10^{-9}	0.52	1.32×10^{8}	98.1

3.5. The polarization curves test

Electrochemical measurements were used to estimate the electrochemical parameters associated with the corrosion process occurring on the substrate covered with different films during immersion time [39]. It was generally recognized that a lower corrosion current density and higher corrosion potential corresponded to a better corrosion resistance. Fig.8 depicted the potentiodynamic polarization curves for different samples. It could be found that the corrosion current density was changed after being treated by the protective technologies. Al alloy with anodic oxide film and sol-gel film had much better corrosion resistance than the blank samples. For LBL sample, the current density was only 0.00316 μA/cm^2, which was two orders of magnitude lower than that of the other samples, and the open circuit potential was 0.31V, which was 200mv higher than that of sol-gel sample and 400mv higher than that of the other two samples. Therefore, the LBL film was beneficial to repel and isolate corrosion medium from attaching to the substrate due to the pores and discharge channels were blocked by it [40], which was in accordance with the results of EIS measurements.

Peer-reviewed version available at Materials 2019, 13, 111; doi:10.3390/ma13010111

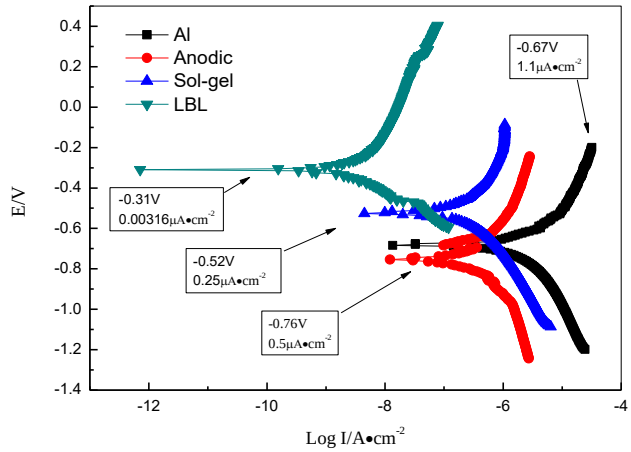

Figure 8. Polarization curves of Al alloy, anodic oxide film, sol-gel film and LBL film.

3.6. Salt spray tests

The traditional neutral salt spray tests were used to estimate protection performance for different films. Surface morphology of different samples after salt spray test for 168 h were depicted in Fig.9. There were many cracks appeared obviously on the surface of blank Al alloy, as shown in Fig. 9a. The surface of blank Al alloy sample were covered with large and loose products, looking like an irregular mass or cell shape. The products increased in the thickness and spread outward to form a large area of erosion with time. Four elements, such as Al, Cl, O and Na, were detected in the corrosion products, indicating that the aluminum oxide film was too fragile to withstand the invasion of chloride ions. Pitting corrosion was too easy to occur for this kind of materials.

For Al alloy covering with anodic oxide film, the surface was also not smooth, and some micro-cracks could be observed (Fig.9b) after salt-spray test. But the number of pitting pits was less than that of blank Al alloy, and the cracks were tiny and distributed evenly. It indicated that when the anodic oxide film was put in the environment including chloride ions, the corrosion process would initiate from the weak grain boundary gradually and outwardly. According to the results of EDS analysis, the white corrosion product was aluminum chloride or carbide, which might be due to the fact that the anodic oxide film was a typical porous structure. The Al alloy matrix was invaded rapidly by chloride ions through the pore structure to caused corrosion. With the accumulation of corrosion products and prolonging of corrosion time, the protective effect of the anodic oxide film was reduced. The porous structure of the anodic oxide film had a high adsorption capacity to trigger corrosion by absorbing moisture, salt, and corrosive media in the surrounding environment. Therefore, the anodic oxide film should be sealed to improve the corrosion resistance.

Surface morphology of the sol-gel films after salt spray test for 168 h were depicted in Fig.9c. Some microcracks accompanied with nubby bumps appeared on the surface of the samples. But the width and depth of cracks were significantly lower than those of blank Al alloy and the anodic oxide film after salt spray test. According to the results of EDS analysis, the content of Cl element on the surface was only 2.97 %, indicating that the salt spray corrosion was partly prevented by the sol-gel film and did not penetrate into the matrix. Although the sol-gel film was uniform and dense, there were still fine pores in macroscopic morphology. Because the radius of chloride ion was much less than the breadth of the cracks, they would easily penetrate into the substrate. Therefore, these defects of the sol-gel film under salt spray conditions made it unable to withstand the salt fog erosion for a long-term, so, the sol-gel film was also needed further treatment by other technologies.

Peer-reviewed version available at Materials 2019, 13, 111; doi:10.3390/ma13010111

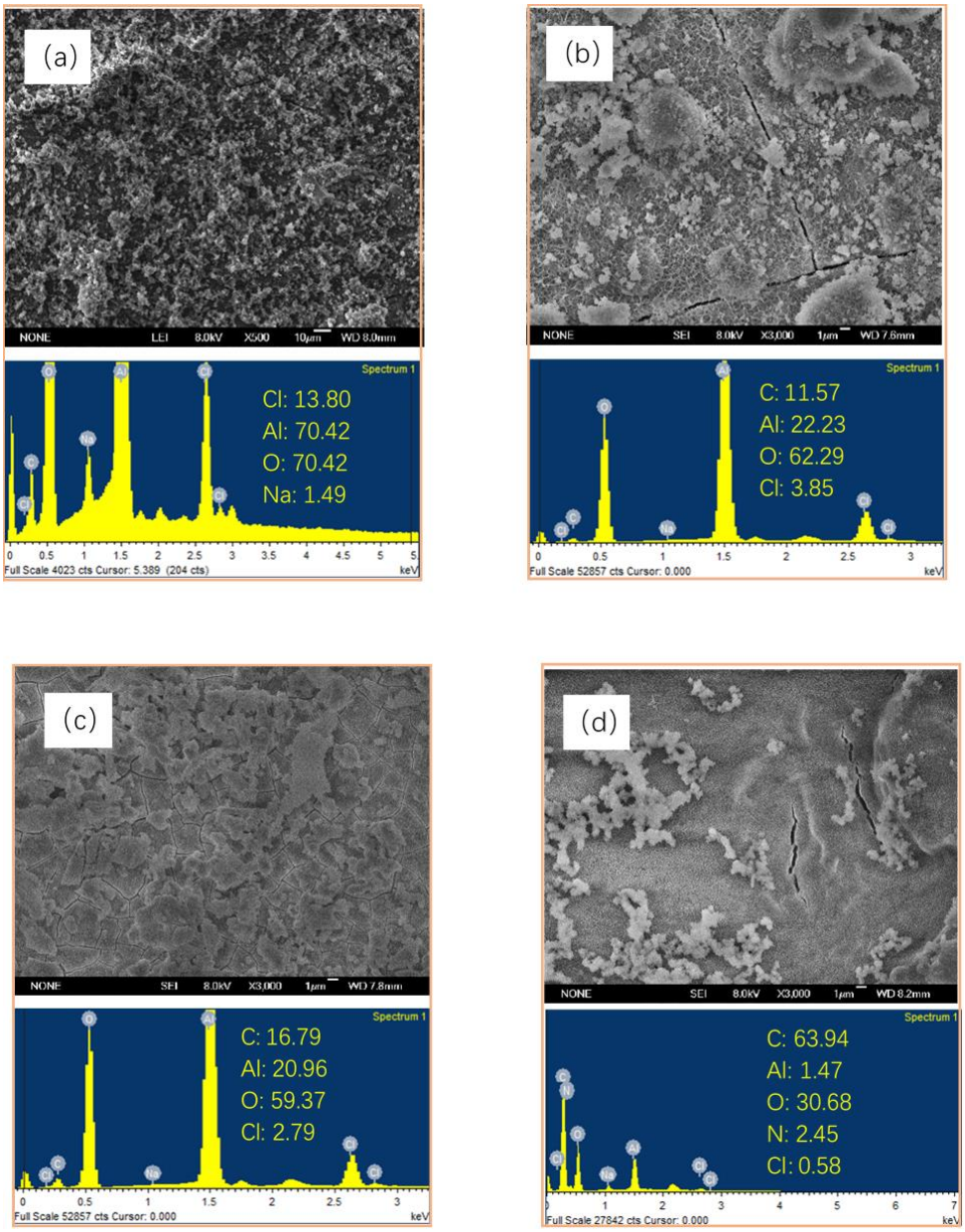

Figure 9. The surface morphology of (a)blank Al alloy, (b) Anodic oxide film, (c)Sol- gel film, (d)LBL film, and EDS images after salt-spray test for 168h.

From Fig.9d it can be seen that the corrosion degree of LBL film was light, comparing with the other samples. The surface of LBL film had high uniformity and smoothness from the macroscopic view. Less corrosion products and defects were found on the surface. The main elements for LBL film after salt-spray test for 168h were C and O. The content of Cl and Al were only 0.58 % and 1.47 %, respectively. Almost no chloride ions adhered on the surface, and the substrate of aluminum was not corroded during the process of salt spray test. Therefore, it could be concluded that the as-prepared LBL self-assembled film covered ideally on the surface of sol-gel film, blocking the eroding path of corrosive medium and improving the corrosion resistance of Al alloy.

4. Conclusions

In summary, a multilayered coating was successfully fabricated on 2A12 aluminum alloy surface combining anodization, sol-gel and LBL strategies. The anodic oxide film and sol-gel film can improve the anticorrosive abilities of Al alloy, with the charge transfer resistant increased by one or two orders of magnitude comparing to the blank Al alloy. However, the cracks were still observed in these two films after analyzed by SEM and EIS, which would affect

Peer-reviewed version available at Materials 2019, 13, 111; doi:10.3390/ma13010111

the long-term protective ability for Al alloy. LBL layer, which was proved to own good sealing performance, could fill the pores and cracks effectively and improve the anticorrosion ability of Al alloy with the coating resistance as high as 9.03×10^6 Ω cm^2 and the system impedance is higher than 10^8 Ω cm^2. After salt-spray test, the film, which was prepared by LBL method, exhibited the best protective ability with less defects and good surface state. It was believed that this kind of multilayers would have broad application and bright prospect in marine corrosion and protection.

Acknowledgments: This work was financially supported by Key R & D projects in Shandong(GG201709260036), National key R & D projects（2017YFB0903702）and the Chinese National Natural Science Foundation (NSF) Grant No. 51678318. All these supports are gratefully appreciated.

Conflicts of interest: All the authors declares that there are no conflicts of interest exist.

References

1. E.S.M. Sherif, H.R. Ammar, K.A. Khalil (2014) Effects of copper and titanium on the corrosion behavior of newly fabricated nanocrystalline aluminum in natural seawater, Appl Surf Sci 301:142-148.
2. Huang Y, Shih TS, Chou J (2013) , Electrochemical behavior of anodized AA7075-T73 alloys as affected by the matrix structure, Appl Surf Sci:283 249-257.
3. Savaskan T and Murphy S (1984) Comparative wear behavior of Zn-Al based alloys in an automotive engine application, Wear, 98:151-161.
4. Jian H, Yin Z, Jiang F, Li X and Nonfer T(2014) EBSD analysis of fatigue crack growth of 2124 aluminum alloy for aviation, Rare Met Mater Eng 43: 1332-1336.
5. Kotov AD, Mikhaylovskaya AV, Kishchik MS, Tsarkov AA, Aksenov SA and Portnoy VK (2016) Near net shape casting process for producing high strength 6xxx aluminum alloy automobile suspension parts, J Alloys Compd 688: 336-344.
6. Rac A, Babic M, Ninkovic R and Balk J(2001) Theory and practice of Zn-Al sliding bearings, J Balk Tribol Assoc 7: 234-240.
7. Babic M and Ninkovic R(2004) Zn-Al alloys as tribomaterials, Tribol Ind 26: 3-7.
8. Babic M, Ninkvoic R and Rac A(2005) Sliding wear behavior of Zn-Al alloys in conditions of boundary lubrication, The Annals of University "Dunarea De Jos" of Galati Fascicle VIII, Tribology, 60-64
9. Lu Z, Wang P, Zhang D (2015) Super-hydrophobic film fabricated on aluminium surface as a barrier to atmospheric corrosion in a marine environment, Corros Sci 91287-296.
10. Vera R, Delgado D and Rosales BM (2006) Effect of atmospheric pollutants on the corrosion of high power electrical conductors: Part 1. Aluminum and AA6201 alloy, Corros Sci 48: 2882-2900.
11. Hou BR, Li XG, Ma XM, Du CW, Zhang DW, Zheng M, Xu W, Lu D, Ma FB(2017) The corrosion coat of China, npj Materials Degradation, 1: 4.
12. Mayén J and Abúndez A(2017) Correlation between mechanical properties and corrosion behavior of an Al 6061 alloy coated by 5% CH_3COOH pressurized steam and RRA heat treated, Surf Coat Technol 309:344–354.
13. Abidi F, Savaloni H(2017) Surface nanostructure modification of Al substrates by N+ ion implantation and their corrosion inhibition, Trans Nonferrous Met Soc China 27: 701−710.

Peer-reviewed version available at Materials 2019, 13, 111; doi:10.3390/ma13010111

14. Ou J, Hu W, Xue M, Wang F and Li W(2013) Superhydrophobic surfaces on light alloy substrates fabricated by a versatile process and their corrosion protection, ACS Appl Mater Interfaces 5: 3101-3107.
15. Caubert F, Taberna PL and Arurault L (2016) Innovating pulsed electrophoretic deposition of boehmite nanoparticles dispersed in an aqueous solution, into a model porousanodic film, prepared on aluminum alloy 1050, Surf Coat Technol 302: 293-301.
16. Hashimoto T, Zhou X, Skeldon P and Thompson GE (2015) Structure of the copper-enriched layer introduced by anodic oxidation of copper-containing aluminum alloy, Electrochim Acta 17: 9394-401.
17. Zhang X and Chen W (2015) Review on corrosion-wear resistance performance of materials in molten aluminum and its alloys, Trans Nonferrous Met Soc China 25: 1715–1731.
18. Thaia TT, Druarta ME, Paintc Y, Trinhb AT and Olivier MG (2018) Influence of the sol-gel mesoporosity on the corrosion protection given by an epoxy primer applied on aluminum alloy 2024 –T3, Prog Org Coat 121: 53-63.
19. Yan R, He W, Zhai T and Ma H(2019) Anticorrosion organiceinorganic hybrid films constructed on iron substrates using self-assembled polyacrylic acid as a functional bottom layer, Electrochimi Acta 295: 942-955.
20. Poorteman M, Renaud A, Escobar J, Dumas L, Bonnaud L, Dubois P and Olivier MG(2016), Thermal curing of paraphenylenediamine benzoxazine for barrier coating applications on 1050 aluminum alloys, Prog Org Coat 97: 99-109.
21. Zheludkevich ML, Salvado IM and Ferreira M (2005) Sol-gel coatings for corrosion protection of metals, J Mater Chem 15: 5099-5111.
22. Wankhede RG, Morey S, Khanna AS, Birbilis N(2013), Development of water- repellent organiceinorganic hybrid solegel coatings on aluminum using short chain perfluoro polymer emulsion, Appl Surf Sci 283: 1051-1059.
23. Habazaki H, Kimura T, Aoki Y, Tsuji E, Yano T (2014) Highly enhanced corrosion resistance of stainless steel by sol-gel layer-by-layer aluminosilicate thin coatings, J Electrochem Soc 161: C57-C61.
24. Kim JS, Kand TH and Kim IK (2009), Surface treatment to improve corrosion resistance of Al plate heat exchangers, Trans. Nonferrous Met Soc China 19: 28-31.
25. Chen D and Zheng J (2002) Advances in technology of preparing anti-corrosion ceramic coating on metal surface with sol-gel process, Mater Rev 16: 28
26. Ohmori A, Li C J (1993), The structure of thermally sprayed ceramic coatings and its dominant effect on the coating properties, Plasma spraying, Theor Appl 179-200.
27. Zhao X, Jin Z, Zhang B et al (2017) Effect of graphene oxide on anticorrosion performance of polyelectrolyte multilayer for 2A12 aluminum alloy substrates, RSC Adv 7:33764-33774.
28. Zhao Y, Shi L, Ji X, Li J, Han Z, Li S, Zeng R, Zhang F and Wang Z (2018) Corrosion resistance and antibacterial properties of polysiloxane modified layer-by-layer assembled self-healing coating on magnesium alloy, J Colloid Interf Sci 526: 43-50.
29. Skorb EVand Andreeva DV(2013), Layer-by-Layer approaches for formation of smart self-healing materials, Polym. Chem. 4: 4834-4845.

Peer-reviewed version available at Materials 2019, 13, 111; doi:10.3390/ma13010111

30. Carneiro J, Caetano A, Kuznetsova A, Maia F, Salak A, Tedim J, Scharnagl N, Zheludkevich M and Ferreira M (2015), Polyelectrolyte-modified layered double hydroxide nanocontainers as vehicles for combined inhibitors, RSC Adv 5: 39916–39929.
31. Liu P, Cai K, Yang W(2012) Improved anticorrosion of magnesium alloy via layer-by-layer self-assembly technique combined with micro-arc oxidation, Mater Lett 75:118–121.
32. Decher G (1997) Fuzzy nanoassemblies: toward layered polymeric multicomposites, Science 277:1232–1237.
33. Li D (2008) Influence of surface dislocation and scratch of purity aluminum crystals on the initiation of pit etching. University of Science and Technology Beijing, Beijing
34. Zhang B, Zhao X, Li Y, and Hou B (2016) Fabrication of durable anticorrosion superhydrophobic surfaces on aluminum substrates via a facile one-step electrode position approach, RSC Adv 6:35455-35465.
35. Zhao X, Wang J, Li W, Hou B (2011). Research on coating deterioration process under fully immersing condition by using multi-parameters, Mater corros 5: 431-435.
36. Wang P, Zhang D, Qiu R and Wu J (2014) Super-hydrophobic metal-complex film fabricated electrochemically on copper as a barrier to corrosive medium, Corros Sci 83: 317-326.
37. Zhao X, Wang J, Wang Y, Kong T, Zhong L, Zhang W (2007) Analysis of deterioration process of organic protective coating using EIS assisted by SOM network, Electrochem Commun 9: 1394-1399.
38. Zhang BB, Guan F, Zhao X, Zhang YM et al (2019) Micro-nano textured superhydrophobic 5083 aluminum alloy as a barrier against marine corrosion and sulfate-reducing bacteria adhesion, J TsiWan Inst Chem E 97: 433-440.
39. Xue B, Yu M, Liu J, Liu J, Li S, Xiong L(2017), Corrosion protection of AA2024-T3 by sol-gel film modified with graphene oxide, J Alloy Compd 725: 84-95.
40. Zhao X, Liu S, Wang X and Hou BR(2014), Surface modification of ZrO_2 nanoparticles with styrene coupling agent and its effect on the corrosion behavior of epoxy coating, Chin J Oceanol Limnol, 32: 1163-1171.